EDMS Document Number: **2810101**
Rev: 1.0- Status: Released

ORGANISATION EUROPEENNE POUR LA RECHERCHE NUCLEAIRE
EUROPEAN ORGANIZATION FOR NUCLEAR RESEARCH
Laboratoire Européen pour la Physique des Particules
European Laboratory for Particle Physics

Occupational Health & Safety and Environmental Protection Unit

Technical Note
27 December 2022

Correction factor for the number of incident protons using correlation between SEC1 and PMIEA822 radiation monitor in the CHARM during Run2.

prepared by:	**verified by:**	**approved by:**
A. E. Lee (KEK)	B. A. Infantino (HSE-RP)	C. R.Froeschl (HSE-RP)
D. T. Sanami (KEK)		E. T. Sanami (KEK)
F. N. Shigyo (Kyushu Univ.)		
G. T. Kajimoto (Hiroshima Univ.)		

CERN-OPEN-2023-005
27/12/2022

Summary

In the CHARM facility, the beam intensity is obtained from the counts in the secondary emission chamber, denoted as SEC1. However, the SEC1 shows the nonlinear counting efficiency when the beam intensity was lower than around 1×10^{11} proton per pulse. The beam intensity could be varied from 1×10^{9} to 5×10^{11} proton per pulse. Due to the nonlinearity of the SEC1 counting efficiency, the conversion to the number of incident protons is not applicable in the low beam intensity region around 10^{9} protons per pulse. Thus, an air-filled plastic ionization chamber (PMIEA822 radiation monitor), which is installed in the irradiation room, is used to determine the correction factor that is used for compensating the nonlinear effect of the SEC1 for low-intensity proton beam. The correction factor was determined by checking the ratio of the readings from the PMIEA822 radiation monitor to the SEC1. In this report, the number of incident protons was analytically corrected with the correlation between SEC1 and PMIEA822 radiation monitor. The corrections were applied by multiplying the correction factors with the beam intensity determined by the SEC1 counts.

Modifications

Revisions	Date	Pages	Description
1.0	20. 12. 2022	all	Creation of document

Contents

1 Introduction **4**

2 Beam monitoring **5**

2.1 Beam Specification 5

2.2 Instrumentation 5

2.3 Operation conditions 5

3 Analysis **8**

3.1 Data points 8

3.2 Grouping 10

3.3 Calibration parameters by data fitting 14

3.4 Uncertainty 15

3.5 Correction factor 16

3.6 Comparison with activation foil 17

4 Conclusions **18**

Acknowledgments **19**

References **19**

1 Introduction

High-energy mixed radiation field is created at a high-energy and high-intensity hadron accelerator by the intended interaction of the beam with a target, beam dump, and collimator and by unintended beam loss point on structural components of the machine. This field is characterized by ionizing radiation, e.g. γ-ray, β-ray, and particle radiation, and a wide range of energies up to TeV. Exposure to ionizing radiation affects all work at the accelerators and in the associated experimental facilities. The average energy of these radiation increase as the beam intensity increase, making them capable of generating further inelastic interaction. In terms of radiation protection, radiation fluence and dose play an important role in the estimation of exposure to ionizing radiation. The fluence and dose are normalized to the number of incident particles in order to be quantified. Thus, a more accurate number of incident particles is required.

The CERN High energy AcceleRator Mixed field facility (CHARM) is located in the East Experimental Area that receives beam from the CERN Proton Synchrotron (PS). The aim of this facility is to provide test locations for electronics and systems in the well-characterized mixed radiation field in order to study the effect of radiation on the components. Thus, there are a number of experimental studies, which have already been done with a variety of configurations in response to the radiation field requirements of the users.

In the CHARM facility, the number of incident protons arriving at the target is obtained by the counts in the secondary emission chamber, denoted as SEC1. The SEC1 is installed upstream of the IRRAD facility [1]. The calibration factor of SEC1, 1.87×10^7 protons per count, has been converted into the counts per pulse to obtain the number of protons per pulse. The calibration factor was determined experimentally from the induced activity of aluminum foil by proton beam irradiation [2]. This calibration factor was determined for maximum proton beam intensity of 5 $\times 10^{11}$ protons per pulse. However, due to the nonlinearity of the SEC1 counting efficiency, the conversion is not applicable in the low beam intensity region around 10^9 protons per pulse. On the other hand, an air-filled plastic ionization chamber, denoted as the PMIEA822 radiation monitor, is installed at the side wall of the CHARM irradiation room. The beam intensity is monitored with the SEC1 and as well by the PMIEA822 radiation monitor. (Note: the PMIEA822 radiation monitor, which is originally planned for monitoring the radiation dose in the CHARM irradiation room, can provide relative information on the beam intensity.) Thus, the PMIEA822 radiation monitor can be used to determine the correction factor that is for compensating the nonlinear effect of the SEC1 for low-intensity proton beam. The correction factor was determined by checking the ratio of the readings from the PMIEA822 radiation monitor to the SEC1. The readings were recorded pulse by pulse and their stability was confirmed during each data-acquisition run. The correction of nonlinearity depends on the beam intensity. The correction factor increased with decreasing number of protons per pulse.

In this report, the number of incident protons was analytically corrected with the correlation between SEC1 and PMIEA822 radiation monitor. The corrections were applied by multiplying the correction factors with the beam intensity determined by the SEC1 counts. From this correction, when the SEC1 stops counting abruptly, the beam intensity can be estimated through interpolation from PMIEA822 data only.

2 Beam monitoring

2.1 Beam Specification

The CHARM facility receives a pulsed proton beam with a momentum of 24 GeV/c from the CERN PS. The beam intensity could be varied from 1×10^9 to 5×10^{11} protons per each beam pulse. The beam is structured in the spill (pulse) with a pulse length of several hundreds of milliseconds. The maximum average intensity of the proton beam was 6.7×10^{10} protons/s.

2.2 Instrumentation

The beam intensity was monitored with the SEC1 and PMIEA822 radiation monitor. A diagram of the beam instrumentation used for the beam line [3] is shown in Figure 1. The SEC1 is installed upstream of the IRRAD facility. When the proton beam crosses the SEC1, the secondary emission of electrons from the surface occurs. The PMIEA822, located in the CHARM irradiation room, is exposed to high-energy particles occurring close to the target.

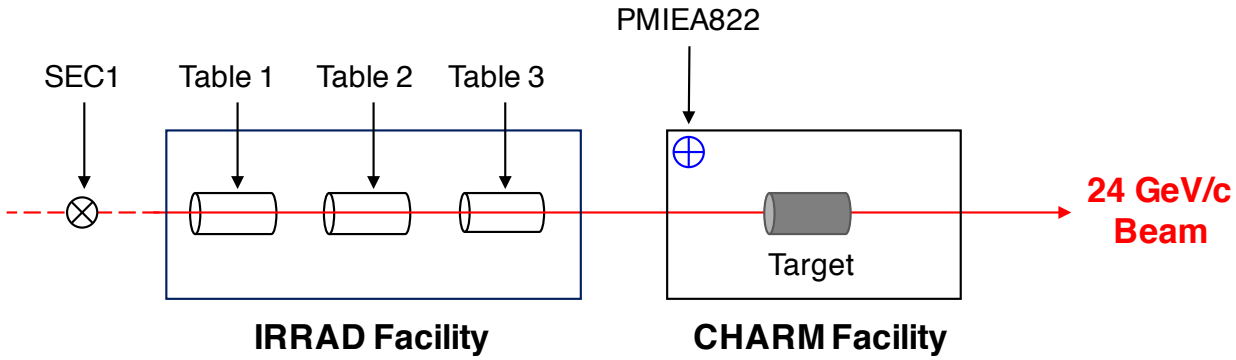

Figure 1: A diagram of the beam instrumentation for the beam line.

The SEC1 measures the energy deposition by the beam in the matter and is usually used for the intensity of high-energy proton beam above a few hundred pA [2]. (Note: The average beam current of the CHARM facility corresponds to 10.7 nA for maximum average beam intensity of 6.7×10^{10} protons per second.) The PMIEA822 is filled with air. Air elements inside the PMIEA822 are irradiated with secondary particles generated from high-energy hadronic interactions. All data from the SEC1 and PMIEA822 were continuously logged in the CERN Accelerators Logging Service (CALS) and extracted through the TIMBER interface. The three irradiation tables of the IRRAD facility shown in Figure 1 can automatically remove the irradiation samples during the nominal CHARM facility operation.

2.3 Operation conditions

The beam intensity taken from the beam instrumentation were obtained in 2016, 2017, and 2018, when a series of shielding experiments have been conducted. The beam operations have different

conditions depending on which beam intensities are required in the measurement. Figures 2,3,4 show histories of both the SEC1 counts and the readings of PMIEA822 during the shielding experiment for FY16, FY17, and FY18, respectively. The black points indicate the radiation dose rate measured by the PMIEA822 radiation monitor, binned in 10 seconds long intervals. The red points indicate the detector counts per pulse measured by SEC1. The heights of the points on the plot represent the values proportional to the beam intensity.

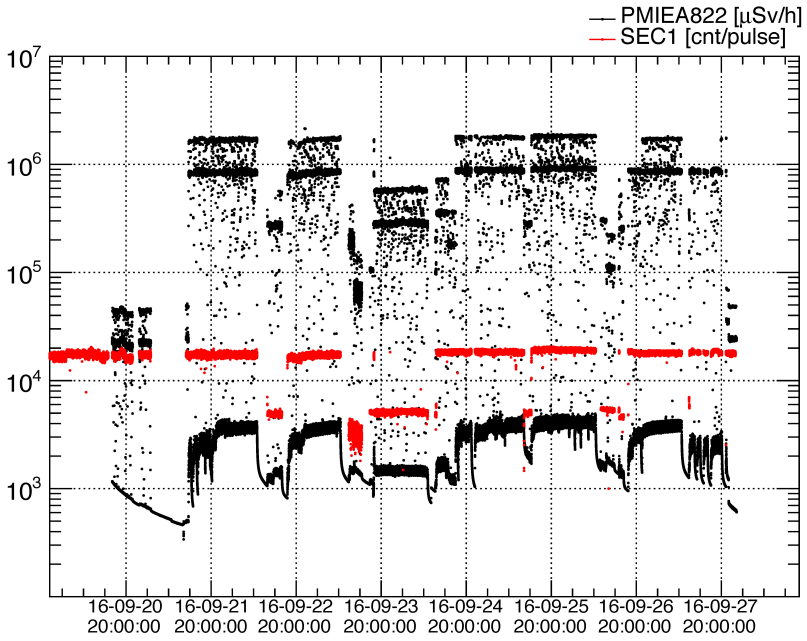

Figure 2: Histories of both the SEC1 counts and the readings of PMIEA822 during the shielding experiment in FY16.

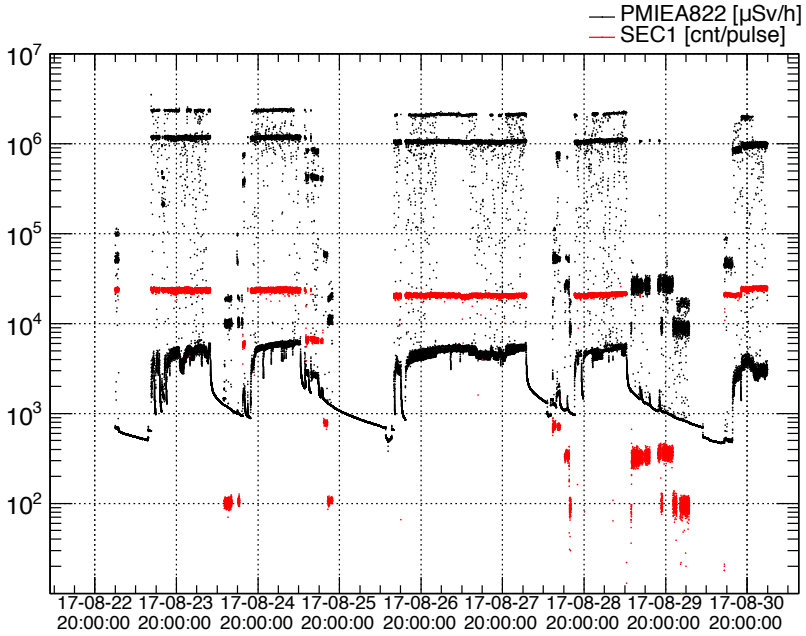

Figure 3: Histories of both the SEC1 counts and the readings of PMIEA822 during the shielding experiment in FY17.

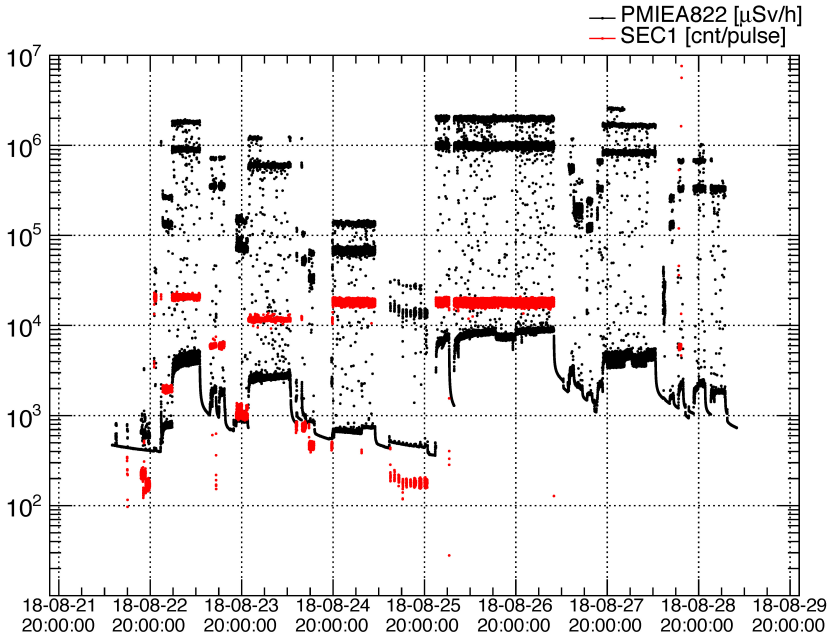

Figure 4: Histories of both the SEC1 counts and the readings of PMIEA822 during the shielding experiment in FY18.

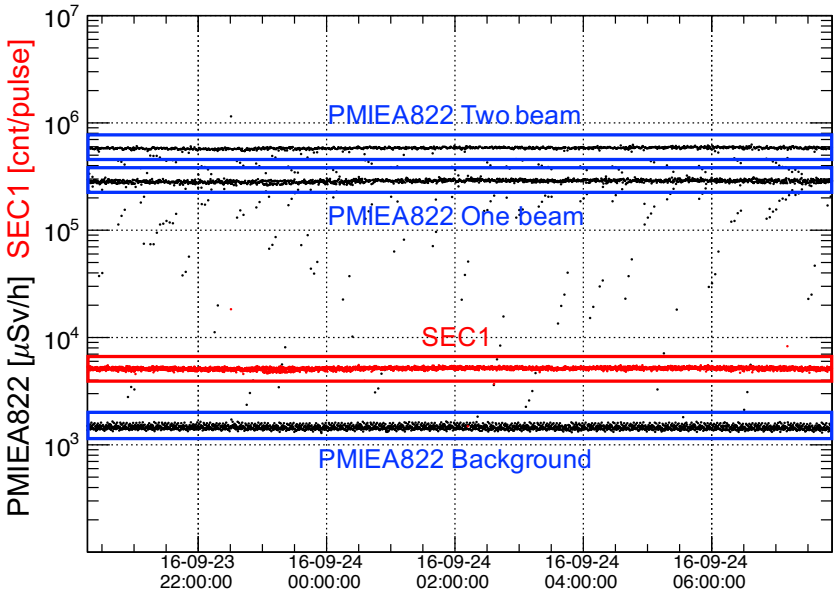

Figure 5: Enlarged portion of Figure 2 to view the full details.

3 Analysis

3.1 Data points

As shown in Figure 5, data can be classified as SEC1 region, one beam (PMIEA822) region, two beams (PMIEA822) region; whose dose rate is nearly twice as much as the one beam with every few seconds, and background (PMIEA822) region. In order to extract data points for the calibration procedure, each region was sorted according to the time basis of SEC1 for dividing each section. That is, the data points can be represented by equation (1).

$$\left.\begin{aligned} \text{Data points} : & \underbrace{\{x_{1,1}, x_{1,2}, \cdots, x_{1,M_1}\}}_{\text{section 1}}, \underbrace{\{x_{2,1}, x_{2,2}, \cdots, x_{2,M_2}\}}_{\text{section 2}}, \cdots, \underbrace{\{x_{N,1}, x_{N,2}, \cdots, x_{N,M_N}\}}_{\text{section N}}, \\ & N = 1, 2, \cdots, N \\ & M_{\{1,2,\cdots,N\}} = 1, 2, \cdots, M \end{aligned}\right\} \quad (1)$$

where N is the number of sections, M_N is the total number of data points belonged to N-th section, and then x_{N,M_N} is M-th data point on N-th section. Each section contains information about the measurement period. Once the data points are sorted, their mean values are

$$\overline{x}_{\mathrm{N}} = \frac{\{x_{N,1} + x_{N,2} + \cdots, x_{N,M_N}\}}{M_N}, \quad (2)$$

where $\overline{x}_N$ is the average of the data points on the N-th section. The standard deviations σ are also

estimated based on the data points. It follows therefore that

$$X = \{\overline{x}_1, \overline{x}_2, \cdots, \overline{x}_N\},$$
$$S = \{\sigma_1, \sigma_2, \cdots, \sigma_N\}, \tag{3}$$

where X and S are the sets of mean values and standard deviation for section N, respectively. After deducing the mean value, the two beams were subtracted the background and divided by 2, and the one beam was also subtracted the background. Figure 6 shows a plot with data points obtained by the approach mentioned above. In the plot, the SEC1 points provide the coordinates for the y-axis, and the points of one beam and two beams obtained by PMIEA822 provide the coordinates for the x-axis.

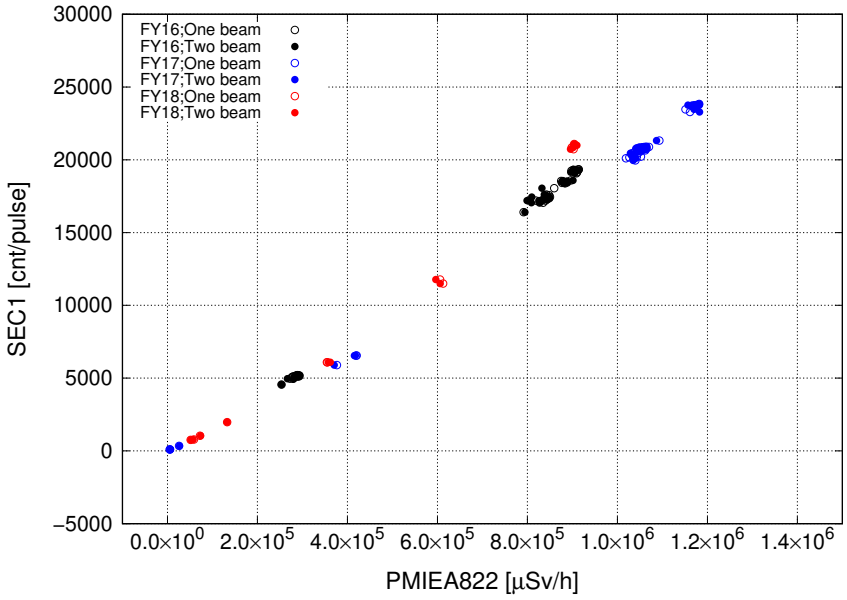

Figure 6: A plot with data points of SEC1 and PMIEA822 radiation monitor.

3.2 Grouping

In order to easily handle the distributed data, the data points were grouped according to similar values within an absolute deviation of 5 %, and it can be defined as follows:

$$\begin{aligned} G_i &= \{\tilde{G}_1, \tilde{G}_2, \cdots, \tilde{G}_i\}, \\ i &= 1, 2, \cdots, I \end{aligned} \tag{4}$$

where I is the number of groups. Due to the varied duration time of measurement, the data points were given different weights depending on their amounts of time. The grouped data points with respect to time ($\tilde{G}_i$), and its standard deviation (σ_{G_i}) were derived based on the following equation:

$$\left.\begin{aligned} \text{grouped data point, } \tilde{G}_i &= \frac{X_{i,1}t_1 + X_{i,2}t_2 + \cdots + X_{i,l_i}t_{l_i}}{t_1 + t_2 + \cdots + t_{l_i}}, \\ \text{standard deviation, } \sigma_{G_i} &= \sqrt{\frac{{S_{i,1}}^2 t_1 + {S_{i,2}}^2 t_2 + \cdots + {S_{i,l_i}}^2 t_{l_i}}{t_1 + t_2 + \cdots + t_{l_i}}}. \\ l &= 1, 2, \cdots, L \end{aligned}\right\} \tag{5}$$

where L is the number of sections included in the i-th group. Additionally, the absolute deviation given in Equation 6 is also reported and its value was used to determine the grouped data points with the acceptable tolerance.

$$\sqrt{(|\frac{X_{i,l_i} - \tilde{G}_i}{\tilde{G}_i}|)^2_{(\text{SEC1})} + (|\frac{X_{i,l_i} - \tilde{G}_i}{\tilde{G}_i}|)^2_{(\text{PMI}-1\text{beam})} + (|\frac{X_{i,l_i} - \tilde{G}_i}{\tilde{G}_i}|)^2_{(\text{PMI}-2\text{beam})}} \times 100(\%) \tag{6}$$

Figures 7,8,9 illustrate the grouping data surrounded by red circle according to similar values for FY16, FY17 and FY18, respectively. No grouping was applied to the data beyond the tolerance of 5% as surrounded by the dotted blue circle. For the sufficient statistics for the low beam intensity region, data points indicated by the dotted black circle were not taken in the data grouping. Note that these are also regarded as respective groups with one point. The uncertainties for data point were derived from relative standard deviation $\frac{\sigma_{G_i}}{\tilde{G}_i} \times 100$ (%), which is used when comparing data with different units of measurement [4] [5]. It can give the information on how much the experimental results are precise and they deviate from the mean value. In other words, the relative dispersion should be used if it is not enough to estimate the dispersion such as the range or variance. Table 1 presents the list of mean value $\tilde{G}_i$, standard deviation σ_{G_i} and uncertainty of data points sorted by grouping.

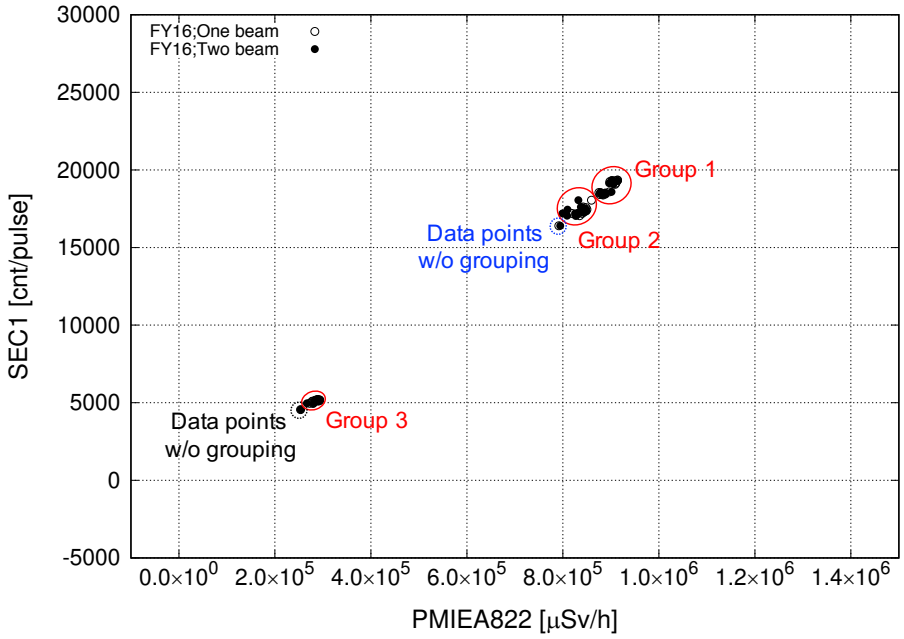

Figure 7: Data grouping according to similar values for FY16.

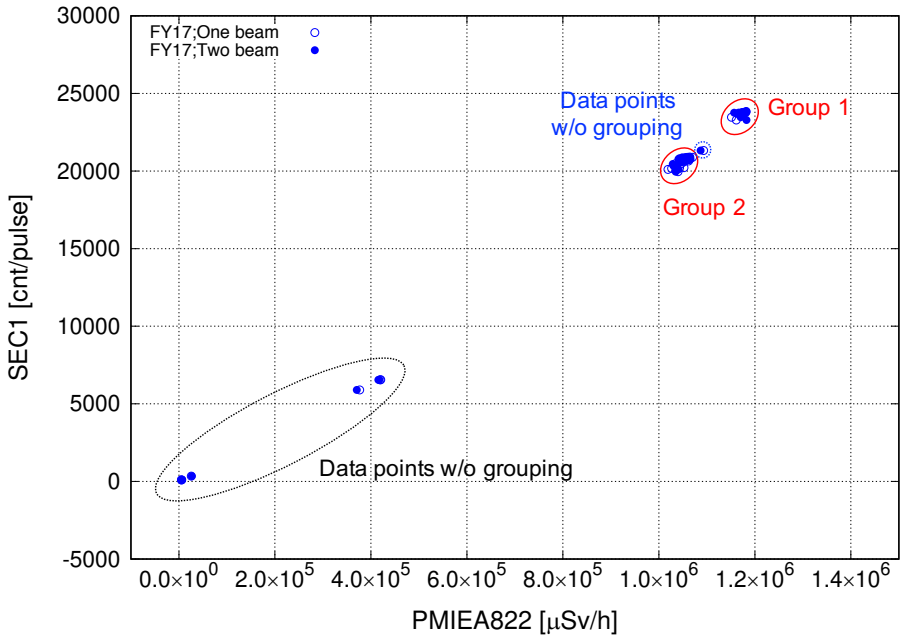

Figure 8: Data grouping according to similar values for FY17.

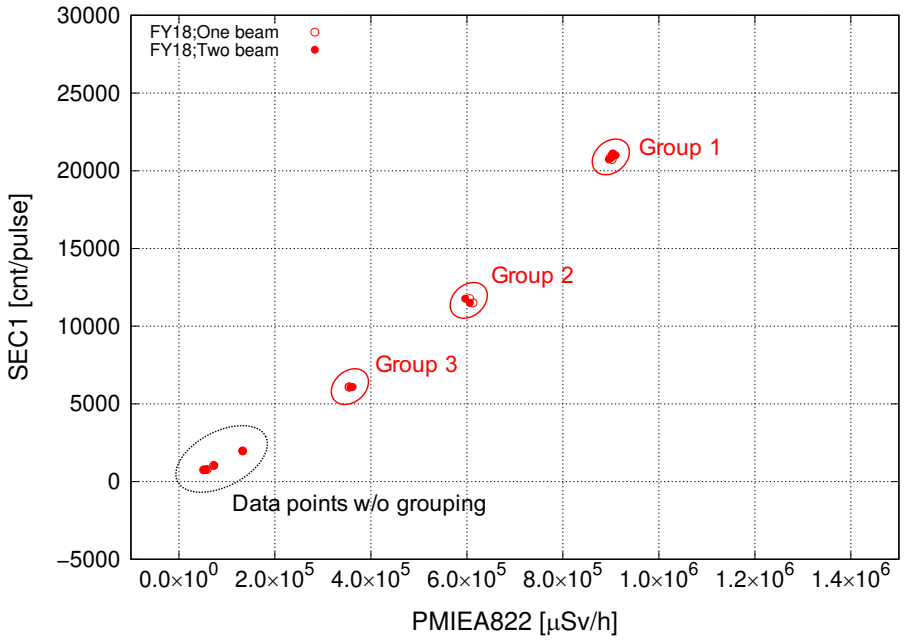

Figure 9: Data grouping according to similar values for FY18.

Table 1: List of mean value $\tilde{G}_i$, standard deviation σ_{G_i} and uncertainty of data points corresponding to SEC1, one beam, and two beams.

	SEC1 [cnt/pulse]			One beam (PMEIA822) [μSv/h]			Two beams (PMEIA822) [μSv/h]		
	$\tilde{G}_i$	σ_{G_i}	Uncertainty (%)	$\tilde{G}_i$	σ_{G_i}	Uncertainty (%)	$\tilde{G}_i$	σ_{G_i}	Uncertainty (%)
FY16									
	1.89E+04	7.60E+02	4.02	8.95E+05	2.89E+04	3.23	8.98E+05	2.81E+04	3.13
	1.75E+04	6.38E+02	3.65	8.40E+05	2.72E+04	3.24	8.26E+05	4.28E+04	5.18
	1.64E+04	6.37E+02	3.88	7.92E+05	3.26E+04	4.12	7.94E+05	2.42E+04	3.05
	5.16E+03	2.61E+02	5.06	2.88E+05	8.40E+03	2.92	2.90E+05	8.79E+03	3.03
	4.96E+03	2.59E+02	5.22	2.73E+05	1.35E+03	0.49	2.69E+05	1.10E+03	0.41
	4.56E+03	9.56E+01	2.10	2.53E+05	5.09E+03	2.01	2.53E+05	9.14E+03	3.61
FY17									
	2.37E+04	1.54E+03	6.50	1.17E+06	3.51E+04	3.00	1.17E+06	3.06E+04	2.62
	2.13E+04	1.17E+03	5.49	1.09E+06	3.00E+04	2.75	1.09E+06	4.33E+04	3.97
	2.06E+04	1.04E+03	5.05	1.05E+06	2.78E+04	2.65	1.05E+06	2.88E+04	2.74
	6.55E+03	5.96E+02	9.10	4.20E+05	1.76E+04	4.19	4.18E+05	1.81E+04	4.33
	6.54E+03	3.23E+02	4.94	4.19E+05	1.88E+04	4.49	4.15E+05	1.14E+04	2.75
	5.89E+03	2.61E+02	4.43	3.77E+05	1.83E+04	4.85	3.70E+05	1.69E+04	4.57
	3.46E+02	2.31E+01	6.16	2.58E+04	1.68E+03	6.51	2.65E+04	6.99E+02	2.64
	1.03E+02	8.37E+00	8.13	5.21E+03	2.85E+02	5.47	6.88E+03	3.83E+02	5.57
	9.31E+01	2.03E+01	21.80	5.23E+03	2.02E+02	3.86	5.81E+03	6.91E+02	11.89
FY18									
	2.09E+04	8.74E+02	4.18	9.02E+05	2.92E+04	3.24	9.03E+05	2.86E+04	3.17
	1.17E+04	6.37E+02	5.44	6.07E+05	1.85E+04	3.05	5.97E+05	2.56E+04	4.29
	6.09E+03	3.05E+02	5.01	3.55E+05	1.25E+04	3.52	3.60E+05	6.94E+03	1.93
	1.97E+03	7.31E+01	3.62	1.33E+05	5.15E+03	3.87	1.33E+05	4.07E+03	3.06
	1.04E+03	1.09E+02	10.48	7.23E+04	5.00E+03	6.92	7.37E+04	4.63E+03	6.28
	7.83E+02	3.14E+01	4.01	5.88E+04	2.37E+03	4.03	5.71E+04	2.02E+03	3.54
	7.59E+02	3.70E+01	4.87	5.16E+04	2.41E+03	4.67	5.17E+04	1.55E+03	3.00

3.3 Calibration parameters by data fitting

As mentioned in the introduction, the beam intensity is measured with SEC1 and PMIEA822, and those readings are convenient to determine the correction factor for the counting efficiency. Figure 10 shows the fitting curves of the correlation between the SEC1 and PMIEA822 obtained by the approach mentioned in section 3.1-3. The fitting curves were assumed to be initialized to origin (0,0). A least square approach is typically used to minimize the sum of the squared error for each variable x. As in this approach, uncertainties are often only taken into account on the variable y. In order to include the uncertainties on both x and y, an orthogonal distance regression approach (ODR) was used to estimate the correlation between the two variables x and y by drawing the curve of best fit on the graph. The data points were fitted by a quadratic function. The fitting curves pass through all the given data points. The calibration parameters obtained from the fitting curves were listed in Table 2.

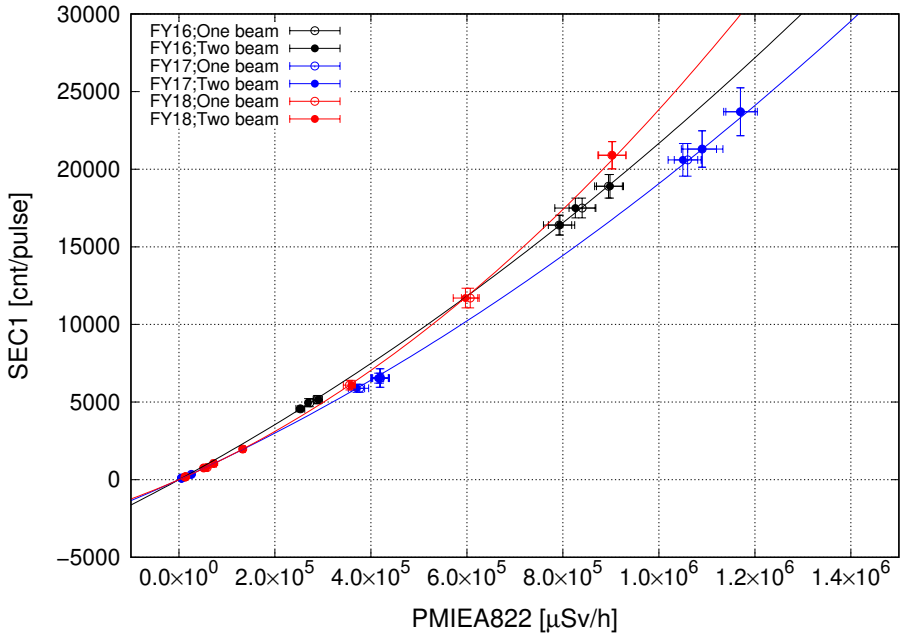

Figure 10: Fitting curve of correlation between the SEC1 and PMIEA822.

Table 2: Calibration parameters obtained from fitting curves to data points

$y = ax^2 + bx$		
	a	b
FY16	4.903E-09	1.677E-02
FY17	5.036E-09	1.403E-02
FY18	1.038E-08	1.346E-02

3.4 Uncertainty

The uncertainties for grouped data were considered based on measured data of the SEC1 counts and the readings of PMIEA822. The average uncertainties corresponding to the SEC1, one beam of PMIEA822, and two beams of PMIEA822 derived from the relative standard deviation as follows [4]:

$$\text{Average uncertainty}(\%) = \sqrt{\frac{\sum_{i=1}^{I}(\frac{\sigma_{G_i}}{\tilde{G}_i})^2}{I-1}} \times 100, \tag{7}$$

where i is the number of groups as mentioned above. Thus, these average uncertainties from measurement were obtained with the help of equation (7) to be 7.20% for SEC1, 4.02% for one beam, and 4.41% for two beams, respectively. The uncertainty of the calibration procedure was estimated by setting uncertainty limits for variable x. Note that variable y is set as a dependent variable of x value in order to set the uncertainty limits. As shown in Figure 11, each area is surrounded by two dotted lines on the left and right sides of the center line. The dotted line of the left side was obtained by connecting lower uncertainties of data points. The dotted line of the right side was obtained in the same manner as the one on the left side using the opposite side of uncertainties. The area formed by the left and right dotted lines based on the center line was referenced as the probable area. The difference between the two dotted lines, namely the uncertainty limits increases as the readings of the PMIEA822 value increase. Table 3 and 4 list the calibration parameters and correction factors obtained from setting the uncertainty limits. The maximum uncertainty limit was estimated to be 3.3% at maximum from the ratio between derived variables $\hat{y}_{\text{center line}}$ and $\hat{y}_{\text{dotted line}}$, which were derived by putting value of x into fitting function. The algorithm describes how to solve the $\hat{y}_{\text{center line}}$ and $\hat{y}_{\text{dotted line}}$ in the section 3.5 later.

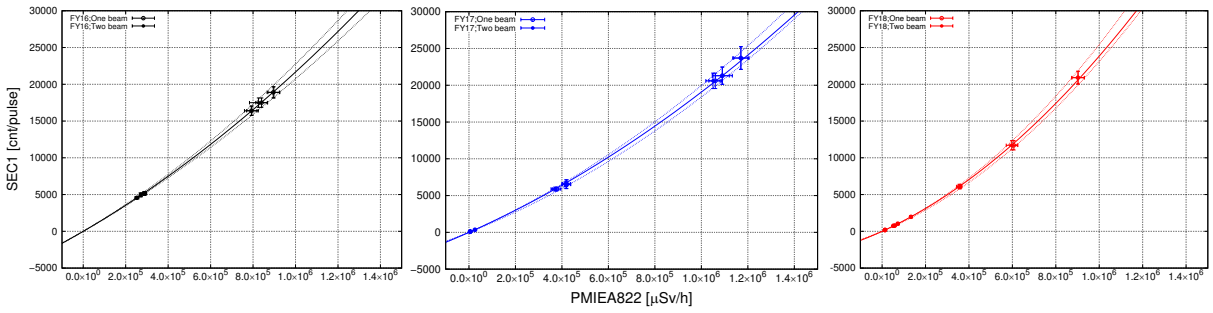

Figure 11: Fitting curve of correlation between the SEC1 and PMIEA822.

The total uncertainty of the beam intensity was estimated to be 9.92% from the propagation of uncertainties as those in the relative standard deviation of the readings from the SEC1 and PMIEA822 and calibration of the correlation between those readings.

Table 3: Calibration parameters obtained from setting the uncertainty limits for each year.

	left side		center		right side	
	a	b	a	b	a	b
FY16	5.727E-09	1.707E-02	4.903E-09	1.677E-02	4.294E-09	1.644E-02
FY17	5.240E-09	1.462E-02	5.036E-09	1.403E-02	5.130E-09	1.319E-02
FY18	1.096E-08	1.401E-02	1.038E-08	1.346E-02	1.007E-08	1.286E-02

Table 4: Correction factors obtained from setting the uncertainty limits for each year.

	SEC1[a] [count/pulse]	No. of protons[b] [proton/pulse]	left side	center correction factor	right side
FY16	1.89E+04	3.53E+11	1.00	1.00	1.00
	1.75E+04	3.27E+11	1.01	1.01	1.01
	1.64E+04	3.07E+11	1.03	1.02	1.02
	5.16E+03	9.65E+10	1.18	1.16	1.15
	4.96E+03	9.28E+10	1.18	1.17	1.16
	4.56E+03	8.53E+10	1.19	1.17	1.16
FY17	2.37E+04	4.43E+11	1.00	1.00	1.00
	2.13E+04	3.98E+11	1.02	1.02	1.03
	2.06E+04	3.85E+11	1.03	1.03	1.03
	6.55E+03	1.22E+11	1.24	1.24	1.26
	6.54E+03	1.22E+11	1.24	1.24	1.26
	5.89E+03	1.10E+11	1.25	1.26	1.28
	3.46E+02	6.47E+09	1.40	1.41	1.46
	1.03E+02	1.93E+09	1.41	1.42	1.47
	9.31E+01	1.74E+09	1.41	1.42	1.47
FY18	2.09E+04	3.91E+11	1.00	1.00	1.00
	1.17E+04	2.19E+11	1.17	1.17	1.17
	6.09E+03	1.14E+11	1.33	1.34	1.35
	1.97E+03	3.68E+10	1.54	1.54	1.56
	1.04E+03	1.94E+10	1.60	1.61	1.64
	7.83E+02	1.46E+10	1.62	1.63	1.66
	7.59E+02	1.42E+10	1.62	1.63	1.66

[a]This SEC1 is data before calibration.
[b]This number of protons is data before calibration.

3.5 Correction factor

After obtaining the calibration parameters, the correction factor was calculated to determine the number of protons. The calculation procedure for correction can be described as in algorithm 1. There are grouped data points, whose value of y increases as the group number i (i = 1, 2, $\cdots$, I) increases. A $\hat{y}_{\tilde{G}_i}$ was set to be maximum value of y, which is defined as $y_{\tilde{G}_i}$. From the Table 2, the inverse fitting function can then produce new value of $\hat{x}_{\tilde{G}_i}$. Similarly, new value of $\hat{x}_j$ can be

obtained by putting y_j into the inverse fitting function (j = 1, 2, $\cdots$, I-1) and then new value of $\hat{y}_i$ is derived as $\hat{y}_{\tilde{G}_i} \times \frac{\hat{x}_j}{\hat{x}_{\tilde{G}_i}}$. Finally, The correction factor α_j can be obtained as $\frac{\hat{y}_j}{y_{\tilde{G}_i}}$.

Algorithm 1 Acquisition of correction factor

1: data points : $(x_{\tilde{G}_1}, y_{\tilde{G}_1})$, $(x_{\tilde{G}_2}, y_{\tilde{G}_2})$, $\cdots$, $(x_{\tilde{G}_i}, y_{\tilde{G}_i})$ (i = 1, 2, $\cdots$, I), $y_{\tilde{G}_1} < \cdots < y_{\tilde{G}_I}$
2: fitting function : $y = f(x)$
3: **Input data : data points, fitting function with calibration parameters**
4:
5: Initialize $\hat{y}_{\tilde{G}_I} = y_{\tilde{G}_I}$, and then $\hat{x}_{\tilde{G}_I} = f^{-1}(y_{\tilde{G}_I})$
6: **for** j = 1, 2, $\cdots$, I-1 **do**
7: $\quad \hat{x}_{\tilde{G}_j} = f^{-1}(y_{\tilde{G}_j})$
8: $\quad \hat{y}_{\tilde{G}_j} = \hat{y}_{\tilde{G}_I} \times \frac{\hat{x}_{\tilde{G}_j}}{\hat{x}_{\tilde{G}_I}}$
9: $\quad \alpha_{\tilde{G}_j} = \frac{\hat{y}_j}{y_{\tilde{G}_j}}$
10: **end for**
11:
12: **Output data :** $(\hat{x}_{\tilde{G}_1}, \hat{y}_{\tilde{G}_1})$, $(\hat{x}_{\tilde{G}_2}, \hat{y}_{\tilde{G}_2})$, $\cdots$, $(\hat{x}_{\tilde{G}_i}, \hat{y}_{\tilde{G}_i})$, $\alpha_{\tilde{G}_j}$

The corrections were applied by multiplying the correction factors with the beam intensity determined by the SEC1 counts as shown in table 4. The correction factor increased with decreasing number of protons per pulse. On the other hand, the correction factor was set to be 1 with the maximum intensity.

3.6 Comparison with activation foil

A experiment using a copper foil activation method for the reaction of ^{nat}Cu(p, X)^{24}Na [6], was conducted to examine the accuracy of the SEC1. The copper foil, whose chemical purity is 99.99+%, with dimensions 50 $\times$ 50 $\times$ 0.02 mm^3 was placed on beam line of the IRRAD facility. The foil was irradiated through 4 runs. All the details of the runs including time of measurement, installation site of Cu activation foil and the average beam intensities defined by the SEC1 during irradiation can be founded in table 5.

Table 5: Count rates of protons measured by the Cu activation foil and the SEC1.

Run No.	Starting time	Ending time	Installation Site of Cu foil	Beam intensity [ppp[a]]
1	08-23-2018 11:30	08-23-2018 15:30	IRRAD	1.12E+11
2	08-23-2018 18:34	08-24-2018 08:49	IRRAD	1.75E+11
3	08-24-2018 10:16	08-24-2018 15:00	IRRAD	2.01E+10
4	08-25-2018 11:02	08-25-2018 20:46	IRRAD	3.39E+09

[a] ppp denotes protons per pulse

Table 6 compares the count rates of incident protons during irradiation time measured by the (a) Cu activation foil, the (b) SEC1 and the (c) corrected SEC1 obtained from the manner mentioned above. The uncertainties for (a) were estimated as 8.7% at maximum. The uncertainties for (b) and (c) were 7.2% and 9.92%, which can be founded in section 3.4.

Table 6: Unit converted data to count per pulse obtained by Cu activation foil, SEC1 and corrected SEC1.

Run No.	(a) Cu foil[a] [cpp[b]]	Unc.	(b) SEC1[c] [cpp]	Unc.	(c) Corrected SEC1 [cpp]	Unc.
1	6.10E+03	5.31E+02	5.99E+03	3.71E+02	8.03E+03	8.11E+02
2	9.77E+03	8.50E+02	9.36E+03	5.80E+02	1.15E+04	1.16E+03
3	1.11E+03	9.66E+01	1.07E+03	6.66E+01	1.73E+03	1.75E+02
4	2.54E+02	2.21E+01	1.81E+02	1.12E+01	3.06E+02	3.09E+01

[a]Data of Cu activation foil and its uncertainties were taken directly from personal communications with T.Oyama.
[b]cpp denotes counts per pulse
[c]This SEC1 is data before calibration.

Table 7: The ratio and its uncertainties of the (b) SEC1 to the (a) Cu activation foil, (b) SEC1 to the (c) corrected SEC1, and the (c) corrected SEC1 to the (a) Cu activation foil.

Run No.	(a)/(b)	Unc.	(c)/(b)	Unc.	(a)/(c)	Unc.
1	1.02	0.11	1.34	0.16	0.76	0.10
2	1.04	0.11	1.23	0.15	0.85	0.11
3	1.03	0.11	1.61	0.19	0.64	0.09
4	1.40	0.15	1.69	0.20	0.83	0.11

As can be seen in tables 5 and 7, as the beam intensity decreases, the ratio of the (b) SEC1 to the (a) Cu activation foil increases. With this tendency, the data of the (c) corrected SEC1 were compared with the (b) SEC1 data in order to confirm the adequacy of the correction factor. If we focus on the lower beam intensity case (run no.4), the ratio of the (b) SEC1 to the (c) corrected SEC1 agrees with those, (a)/(b), within the uncertainty. As was pointed out in section 1, there is a limit to using the calibration factor as it is, in the low beam intensity region around 10^9 protons per pulse.

4 Conclusions

The number of incident protons was analytically corrected with the correlation between the SEC1 counts and the readings of the PMIEA822 radiation monitor. In the CHARM facility, the beam intensity could be varied from 1×10^9 to 5×10^{11}. When the beam intensity was lower than around 1×10^{11} proton per pulse, the SEC1 shows the nonlinear counting efficiency. In order to correct the number of protons, those readings from the SEC and PMIEA822 were used for the correction procedure. The total uncertainty of the beam intensity was estimated to be 9.92% from

contributions in calibration procedures used in this report. The correction factor varied depending on the beam intensity. This procedure can give an estimation of the beam intensity when the SEC1 abruptly stops counting from PMIEA822 data only.

Acknowledgments

The authors would like to thank the participants of this experiment, the CERN Transport Group, the operation staff of the IRRAD and CHARM facilities, and the accelerator operators of the CERN Control Centre for their assistance in the experimental study. We are especially grateful to Marc Delrieux from the Operations Group of the CERN Beams department for setting up a dedicated low intensity slow extraction from the PS to the East Hall for this experiment.

References

[1] J. Mekki and M. Brugger and R. G. Alia and A. Thornton and N. C. D. S. Mota and S. Danzeca. CHARM: A Mixed Field Facility at CERN for Radiation Tests in Ground, Atmospheric, Space and Accelerator Representative Environments. *IEEE Transactions on Nuclear Science*, 63(4):2106–2114, 2016.

[2] A. Curioni and R. Froeschl and M. Glaser and E. Iliopoulou and F.P. La Torre and F. Pozzi and F. Ravotti and M. Silari. Single- and multi-foils 27Al(p,3pn)24Na activation technique for monitoring the intensity of high-energy beams. *Nuclear Instruments and Methods in Physics Research Section A: Accelerators, Spectrometers, Detectors and Associated Equipment 858*, pages 101–105, 2017.

[3] A. Thorton. CHARM Facility Test Area Radiation Field Description. Technical Report CERN-ACC-NOTE-2016-12345, 2013.

[4] Taylor J.R. *An introduction to error analysis*. 2nd. ed. University Science Books, Sausalito, CA, 1997.

[5] D.C. Baird. *Experimentation: An Introduction to Measurement Theory and Experiment Design*. 3rd. ed. Prentice Hall, Englewood Cliffs, NJ, 1995.

[6] S. I. Baker and R. A. Allen and P. Yurista and V. Agoritsas and J. B. Cumming. Cu(p,X)^{24}Na cross section from 30 to 800 GeV. *Phys. Rev. C*, 43:2862–2865, Jun 1991.